Page 1 of 25. © YYYY
doi: 10.1017/aer.2016.1

# Design Study of Coanda Devices for Transonic Circulation Control

**M. Forster**
**mforster@liv.ac.uk**

PhD Student
CFD Lab, School of Engineering
University of Liverpool
UK

**R. Steijl**
**rene.steijl@glasgow.ac.uk**

Senior Lecturer
Aerospace Sciences, School of Engineering
University of Glasgow
UK

## ABSTRACT

Circulation control via blowing over Coanda surfaces at transonic freestream Mach numbers is investigated using numerical simulations. The performance and sensitivity of several circulation control devices applied to a supercritical aerofoil are assessed. Different Coanda devices were studied to assess the effect of; slot height to Coanda radius ratio, nozzle shape, and Coanda surfaces with a step. The range of operating conditions for which a supersonic Coanda jet remained attached at transonic freestream conditions were extended by increasing the radius of curvature at the slot exit for Coanda devices with a converging nozzle. Additional improvements were found by: reducing the strength of shock boundary layer interactions on the Coanda surface by expanding the jet flow using a converging-diverging nozzle, and also by introducing a step between the Coanda surface and the nozzle exit. The performance when using a converging-diverging nozzle can be matched using a simple stepped Coanda device. It is shown that circulation control has the potential to match the performance of traditional control surfaces during regimes of attached flow at transonic speeds, up to an equivalent aileron deflection angle of 10°. In addition, lift augmentation ratios $\Delta C_l/C_\mu$ of over 100 were achieved.

Received 10 10 2016; revised 02 06 2017; accepted 05 06 2017.

# NOMENCLATURE

| | |
|---|---|
| $A$ | Wing Surface Area |
| AOA | Angle of Attack |
| $c$ | Chord Length |
| CC | Circulation Control |
| $C_d$ | Sectional Drag Coefficient |
| CFD | Computational Fluid Dynamics |
| $C_l$ | Sectional Lift Coefficient |
| $C_m$ | Sectional Pitching Moment Coefficient |
| $C_\mu$ | Momentum Coefficient, $\frac{\dot{m}_j U_j}{q_\infty A}$ |
| $C_p$ | Pressure Coefficient |
| $\Delta C_l/C_\mu$ | Lift Augmentation Ratio |
| EXP | Experiment |
| $h$ | Jet Slot Height |
| HMB | Helicopter Multi-Block CFD Code |
| $M$ | Mach Number |
| $\dot{m}_j$ | Jet Mass Flow Rate |
| NPR | Nozzle Pressure Ratio, $P_0/P_\infty$ |
| $P_0$ | Plenum (Total) Pressure |
| $P_\infty$ | Freestream (Static) Pressure |
| $q_\infty$ | Freestream Dynamic Pressure |
| $r$ | Coanda Radius |
| $Re$ | Reynolds Number |
| $s$ | Step Height |
| SARC | Spalart-Allmaras Rotation/Curvature |
| $t$ | Skin thickness |
| TDT | Transonic Dynamics Tunnel |
| UAV | Uninhabited Air Vehicle |
| $U_j$ | Jet Velocity |
| $U_\infty$ | Freestream Velocity Magnitude |
| $y^+$ | Non-Dimensional Wall Distance |

### Greek Symbol

| | |
|---|---|
| $\alpha$ | Angle of Attack |
| $\delta$ | Aileron Deflection |

# 1.0 INTRODUCTION

In aircraft, ailerons have traditionally been used to alter the circulation around the wings for flight control. Flaps employ a similar principle and are used as high lift devices for take-off and landing. An alternative method is circulation control (CC) using the Coanda effect; a jet of air is blown over a rounded trailing edge of a wing. CC using blowing offers advantages over devices such as flaps and ailerons, removing the necessity of moving parts, possibly leading to a reduction in aircraft weight[(1)].

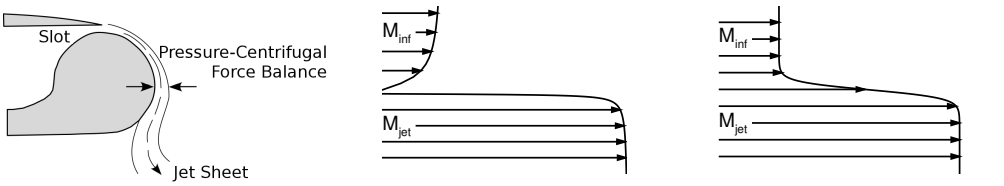


(a) Trailing edge CC[2]. (b) Slot exit flow (c) Shear layer downstream of slot

Figure 1: Schematic of flows at trailing edge.

The Coanda effect describes the behaviour of a fluid moving tangentially to a convex (typically circular) surface. The flow adheres to the curved surface as a result of the pressure gradients within the jet flow (see Fig. 1a). The position of the separation and stagnation points at the trailing and leading edges of the aerofoil are altered due to blowing a jet over the Coanda surface, causing a change in lift.

CC usually requires a high speed jet of air up to 4 times the freestream speed[2], which attaches to the Coanda surface. As this high speed jet meets the relatively lower speed air in the freestream, the jet entrains the fluid within the freestream which is then also turned around the Coanda. The entrainment is due to the mixing within a shear layer between the jet and the freestream travelling at significantly different Mach numbers. Figures 1b and 1c show simplified schematic diagrams of the flows that occur at the slot exit and just downstream of the slot. The momentum of the jet influences the boundary layer and accelerates the local freestream flow.

For aerofoils in the transonic regime, a supersonic Coanda jet is necessary to achieve a significant change in lift. In addition to shear layers there is a possibility of shock boundary-layer interactions occurring on the surface of the Coanda devices, if the jet becomes under-expanded[3]. Depending on the severity of the shock boundary layer interaction, the jet can detach completely from the Coanda surface[4]. At transonic speeds, the shock on the upper surface of the aerofoil also alters the boundary layer flow leading to the CC device at the trailing edge (Fig. 1b), which can affect the behaviour of the Coanda jet flow[5].

For an aircraft to successfully use a CC system it would need to be effective over a wide range of flight conditions, including different altitudes. Changes in altitude as well as engine settings will create differences in the pressure ratio the Coanda device is operating at. Therefore, it is crucial to consider the CC device for a wide range of pressure ratios, mainly a range of conditions with under-expansion and, for cases where a converging-diverging nozzle is used, also over-expansion cases.

Studies on transonic CC have shown that the shape of the Coanda surface plays an important role in the effectiveness of the CC device at transonic speeds[6,7,2,5]. Parameters such as the slot height to (local) Coanda radius ratio affect the attachment of the Coanda jet, and the range of blowing rates (and nozzle pressure ratios) for which the jet remains attached to the Coanda. Experimental investigations into elliptical Coanda surfaces have concluded that more eccentric ellipses and smaller slot heights perform most favourably in transonic flows[6,7,2].

Alternative methods of promoting supersonic Coanda jet attachment have been studied in conditions without a freestream flow. Converging-diverging nozzles have been shown to increase the detachment pressure ratio[8,9] by expanding the jet flow further than a converging

nozzle and limiting under-expansion. The introduction of a step between the Coanda surface and the jet exit of a converging nozzle also increased the detachment pressure ratio[9,8].

There is a lack of research on supercritical CC aerofoils; only subsonic studies have been conducted to date[10]. For this reason, in this work, the performance of a supercritical aerofoil at transonic conditions with a CC device will be investigated. We aim to assess the aerodynamic feasibility of replacing ailerons for transonic flight control on a typical supercritical section. The feasibility of using devices such as converging diverging nozzles and stepped Coanda surfaces for circulation control with a transonic freestream will be investigated. The abilities and limitations of such devices have not previously been considered for transonic circulation control.

In the present work, we focus on the effectiveness of CC devices for a range of nozzle pressure ratios on a supercritical aerofoil in a transonic cruise condition. Comparisons against the characteristics of the supercritical CC aerofoil with an aileron deflection, and also with published experimental results form part of this study. In addition, a design study will be performed to examine the effect of various CC device configurations. We consider the effects of: Coanda radius to slot height ratio, converging-diverging nozzles, and stepped Coanda surfaces , which will be investigated for increasing CC effectiveness for a transonic supercritical CC aerofoil.

Increasing the Coanda radius ($r$) to slot height ($h$) ratio increased the NPR that caused detachment of the jet, with a marginal increase in lift. The use of a simple step was found to extend the NPR and momentum coefficients range for which the jet remains attached. An increase in usable $C_\mu = 0.004$ was found when using the step, this extension increased the lift authority available to the circulation control system by $C_l = 0.1$ compared with a similar device without a step. A converging-diverging nozzle designed for the conditions at which a jet from a converging nozzle with the same $r/h$ separated was found to be equally effective as the stepped Coanda device.

The current paper first reviews related work in CC and supersonic Coanda flows, followed by a description of the numerical methods employed. A validation exercise of the solver against experimental results of a supercritical aerofoil with aileron deflection will be presented. The same aerofoil section was modified into a supercritical CC aerofoil, and forces and moments for blowing over several Coanda devices were compared with those from using an aileron. Finally, a summary of the findings and conclusions are made with recommendations for future research.

## 2.0 REVIEW OF RELATED WORK

CC using the Coanda effect for use as a means of generating an increase in lift over an aerofoil has been in consideration for at least 60 years[11]. Significant focus was invested on improving the lift of rotor blades with elliptical sections amid development of the X-Wing CC concept in the early 1980s[12]. More recently, with concerns over aircraft efficiency and environmental impacts, CC has been studied to improve the lifting capabilities of fixed wing aircraft while keeping within the capabilities of existing airport infrastructures[13]. On fixed wing UAVs, it has been shown in subsonic flight that CC has the potential to replace moving parts for manoeuvrability control[14]. Other active flow control systems are also being studied, such as to allow for a reduction in the vertical tail size of commercial aircraft[15,16].

Much of the CC research to date has investigated flow control devices on aerofoils in the low

speed subsonic flight regime. As a result, modern numerical studies on CC have heavily relied on these subsonic freestream circulation control experiments[17,10,18,19], such as those at the Georgia Tech Research Institute, which were intended specifically for CFD validation and had a trailing edge radius of approximately 10% chord[20]. LDV measurements of the subsonic jet around the Coanda were made with a freestream Mach number of $M = 0.12$. Momentum coefficients up to $C_\mu = 0.150$ were investigated, however it must be noted that $C_\mu$ is inversely proportional to the square of the freestream Mach number via the dynamic pressure. This experiment demonstrated significant wall interference and angle of attack corrections to be suitable for CFD validation simulations[20].

Research on higher speed transonic CC has produced a handful of experiments and numerical studies, which mostly took place in the 1980s on aerofoil sections intended to be used for helicopter blades on the X-Wing CC concept[6,21,22,5]. Such experiments were conducted in moderate size wind tunnels, which introduced significant wall interference effects[23]. The elliptical X-Wing type sections typically had maximum thicknesses of approximately 15% chord, which do not have the characteristics of a supercritical aerofoil, as would be used on a fixed wing aircraft. A supercritical CC aerofoil has been developed[10], however transonic experiments on this section have not yet been published.

The difference between CC at subsonic and transonic speeds is highlighted in Fig. 2, showing the lift obtained by Englar[6] for an elliptical CC aerofoil over a range of Mach numbers. At low speeds, the "Rounded Ellipse" CC aerofoil outperformed the purely elliptical section, however at high speeds this was not the case. Schlecht and Anders[7] found that an elliptical Coanda surface was superior to a biconvex surface for both low subsonic and transonic freestreams, since the separation point of the jet is fixed by the sharp profile of the biconvex Coanda.

Alexander *et. al.*[2] recognised a void in the public domain of data for transonic CC aerofoils, specifically those intended for fixed wing aircraft. A series of experiments were published in 2005 on a 6% thick elliptical aerofoil with a 0.75% circular camber[7] in the NASA Transonic Dynamics Tunnel over a range of Mach numbers up to $M = 0.84$. Three different Coanda designs were considered, each with a range of slot heights. Coanda surfaces with larger major to minor axes performed more favourably than smaller elliptical Coanda surfaces; a greater maximum lift was achieved and detachment of the jet was delayed until higher momentum coefficients. A maximum sectional $\Delta C_l = 0.25$ was achieved at a peak $C_\mu = 0.008$ using an elliptical Coanda device with a $2.98 : 1$ aspect ratio. The same slot height but with a $1.78 : 1$ elliptical Coanda device had a maximum $\Delta C_l = 0.2$ at a peak $C_\mu = 0.005$. Following these peak values a "$C_\mu$-stall" was observed, whereby further increases in blowing reduced $\Delta C_l$ as the jet detached from the Coanda surfaces.

In 2006, Swanson *et. al.*[24] performed two dimensional RANS simulations of the 16% thick, elliptical 103RE aerofoil[21], however the simulations were limited to $M = 0.6$ at $\alpha = 0.0$. At these conditions, the flow over the aerofoil remained subcritical. It was found that each turbulence model tested (Spalart-Allmaras, Menter SST, Spalart-Allmaras with Curvature Correction (SACC) and EASM-$k$-$\omega$) failed to predict the pressure distribution over the aerofoil surface at $M = 0.6$. In addition, the separation point of the jet from the Coanda surface was poorly predicted. The SACC model gave reasonable results but only after unrealistic a-posteriori modifications to the baseline model constants[24]. This highlights that even with modern CFD methods, accurate predictions of CC remain a challenge.

Following the previous numerical studies on transonic CC discussed above, the understanding of the modeling requirements is improving due to increasing capabilities and experience

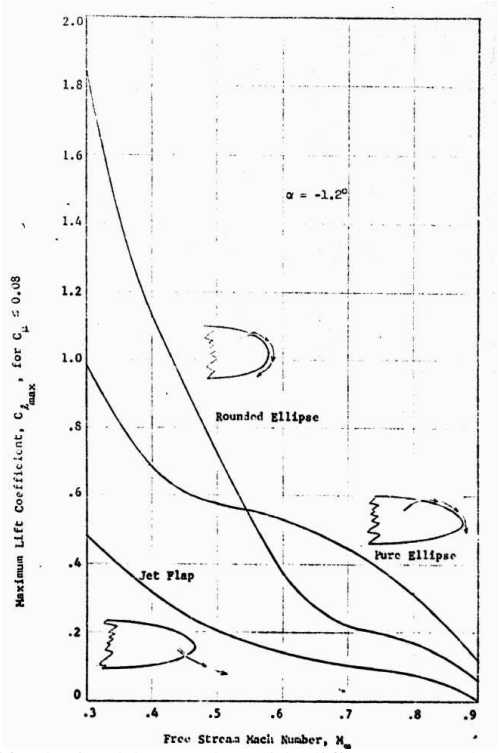


Figure 2: Maximum lift obtained by Englar with different Coanda geometries at range of Mach numbers for $C_\mu \leq 0.08$.[6].

with improved turbulence modelling approaches. Due to the lack of available experimental data for CFD validation of CC at transonic conditions, it is difficult to fully address and identify shortcomings in current CFD approaches. Despite this, however, CFD is the only currently feasible way to conduct a design investigation on CC devices in conditions relevant to transonic flight of aircraft.

To limit the detachment due to under-expansion of the jet, a converging-diverging nozzle can be used to expand the flow to the ambient pressure. In experiments on supersonic Coanda jets in still air, Cornelius and Lucius[25] showed that a simple converging-diverging nozzle extends the range of operating pressures at which the Coanda jet remains attached. Bevilaqua and Lee[26] reported on a method of characteristics design approach which skews the velocity and pressure profile along the jet exit such that the pressure and velocities at the Coanda surface are lower and higher, respectively. Using the radial velocity and pressure profiles of an irrotational vortex at the slot exit, jet attachment was promoted[26].

Other experimental studies have shown that introducing a step between the jet exit and Coanda surface can promote attachment at higher pressure ratios by preventing shock induced separation[8,9]. Carpenter and Smith[8], and Gregory-Smith and Senior[9] have studied the effect of using a step to mitigate the effects of the under-expansion. By introducing a step, the shock waves due to under-expansion interact with the shear layer formed as a result of the step. The step also aids attachment by providing a region of low pressure which turns the jet

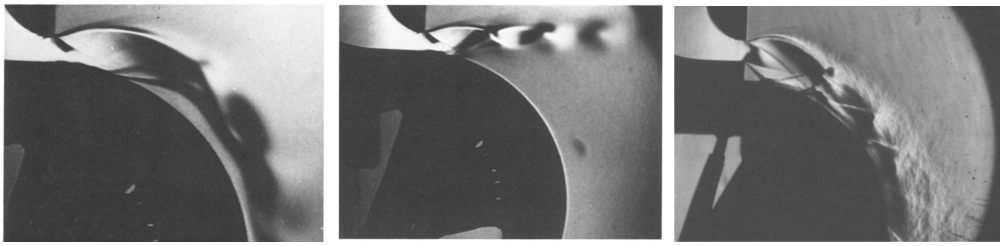

(a) NPR below detachment ratio (b) NPR above detachment ratio (c) NPR above unstepped detachment ratio

Figure 3: Schlieren of unstepped[27] (a and b), and stepped[9] (c) supersonic Coanda jets near detachment.

towards the surface[8]. Figure 3 shows three Schlieren images from experiments by Gregory-Smith *et. al.*[27,9], where the nozzle pressure ratio (NPR) is close to the value at which the jet detached from the surface. Shown in Figs. 3a and 3b are unstepped results before and after jet detachment, an increase in plenum pressure caused the jet to detach. For the same slot height and Coanda radius, including a step increased the detachment pressure ratio by 25%.

Summarising the findings from this review of the literature, we find that all transonic circulation control studies considered previously have been limited to elliptical aerofoil sections. In addition investigations into the effect of different Coanda devices for transonic circulation have essentially only studied the change of curvature at the slot exit. This work instead considered the use of CC on a supercritical aerofoil. We also aim to identify that the use of a stepped supersonic Coanda jet can be used effectively with a transonic freestream.

# 3.0 NUMERICAL METHODS

## 3.1 Navier-Stokes Solver

The Helicopter Multi-Block (HMB) CFD code[28,29,30,31] is used for this work. The code has been validated for a number of applications, including helicopters; wind turbines; turboprops; and high-speed unmanned combat aerial vehicles[31,32,33]. In addition, validation of the solver and boundary conditions for CC has been conducted by Hoholis[34].

HMB solves the compressible, unsteady Reynolds-averaged Navier-Stokes equations on block-structured grids using a cell-centred finite-volume method for spatial discretisation. The convective fluxes are evaluated using Osher's upwind scheme for its robustness, accuracy, and stability properties. MUSCL variable extrapolation is used to provide second-order accuracy with the Van Albada limiter to prevent spurious oscillations around shock waves. An implicit time-integration method is employed, and the resulting linear systems of equations are solved using a pre-conditioned Generalised Conjugate Gradient method. For unsteady simulations, an implicit dual-time stepping method is used, which is based on Jameson's pseudo-time integration approach.

The solver has a library of turbulence closures which includes several one- and two- equation turbulence models[35,36,37,38] and also non-Boussinesq versions of the $k$-$\omega$ model[39,40]. Turbulence simulation is also possible using Large-Eddy and Detached-Eddy Simulation.

### 3.2 Momentum Coefficient

The supply of air for the plenum for circulation control is often taken from bleed air from the jet engine of the aircraft[14]. As a result of this the efficiency of the circulation control device is critical; mass flow taken from the engine reduces the power available for forward thrust. The jet momentum coefficient ($C_\mu$) is often used as a measure of blowing over a circulation control device, which is defined as

$$C_\mu = \frac{\dot{m}_j V_j}{q_\infty A} \quad \ldots(1)$$

where $\dot{m}_j$ is the mass flow rate through the slot exit and $A$ is the surface area of the aerofoil. In circulation control experiments, $\dot{m}_j$ is usually measured using a flow venturi meter and $V_j$ calculated from isentropic equations using the plenum pressure. Here, the plenum pressure ratio is fixed and the momentum coefficient is calculated a posteriori by integrating the solution along the slot exit.

An important and widely used metric for defining the efficiency of a CC system is the lift augmentation ratio $\Delta C_l/C_\mu$. Alexander *et. al.* state that circulation control performance is considered as "good" for $\Delta C_l/C_\mu > 50$[2]. In their experiments on the 6% thick elliptical wing they found a maximum augmentation ratio of 37 for $M = 0.8$. In addition Abramson and Rogers[5] achieved $\Delta C_l/C_\mu = 27$ at $M = 0.7$ and $\Delta C_l/C_\mu = 10$ at $M = 0.8$ on their 16% thick elliptical aerofoil.

### 3.3 Reservoir Boundary Condition

A reservoir boundary condition is used to fix the desired pressure and density ratios based on the assumption that the supply has been isentropically compressed. The stagnation pressure and density are fixed by NPR at the reservoir boundary while velocities at the face are allowed to vary with the condition that no gradients form across the boundary.

Force contributions of pressure and $C_\mu$ from this internal reservoir boundary face are included in the calculation of the total forces and moments, following the approach presented by Min *et. al.*[41]. The pressure and viscous terms are calculated on the external and internal solid surfaces of the wing, while other surfaces such as end plates are excluded. Contributions due to the pressure force and momentum addition of the jet are considered at the reservoir boundary. Figure 4 shows an illustration of the surfaces considered for the calculation of the forces and moments.

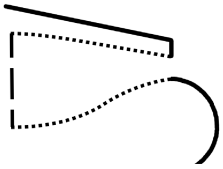

Figure 4: Diagram of trailing edge of circulation control aerofoil. The solid lines are considered as external surfaces, dotted lines are the internal no-slip plenum surfaces and the dashed line is the reservoir boundary condition.

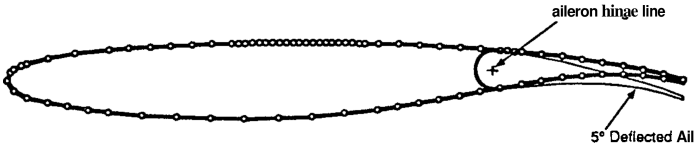


Figure 5: Douglas DLBA032 geometry[42].

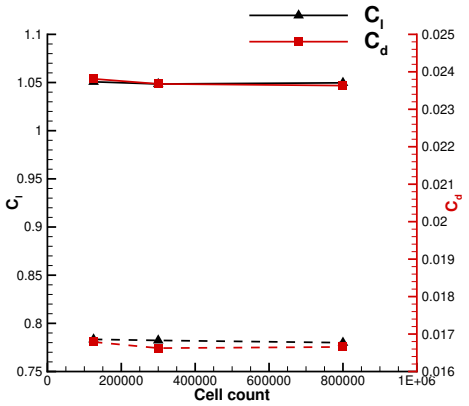


Figure 6: Effect of grid refinement on lift and drag for simulations of the DLBA032 with and without (dashed lines) aileron deflection. Here $M \approx 0.715$, $Re = 5 \times 10^6$ at angles of attack of $\alpha = 1.183°$ with a 3° deflection and $\alpha = 1.342°$ without aileron deflection.

## 4.0 TRANSONIC FLOW OVER A SUPERCRITICAL AEROFOIL WITH AILERON DEFLECTION

The supercritical McDonnell Douglas DLBA032 aerofoil section (Fig. 5) was chosen from the AGARD CFD validation database[42] due to the availability of experimental data with an aileron deflection in a transonic freestream. The DLBA032 is a supercritical aerofoil with a thickness of 12% chord and an aileron of 25% chord length. Experiments were conducted at a Reynolds number range of $Re = 5 \times 10^6$ to $Re = 25 \times 10^6$, an aileron deflection of $\delta = -5°$ to $\delta = 5°$ and $M \approx 0.72$. To promote transition in the experiments, a boundary layer trip was placed at $x/c = 0.15$ and $x/c = 0.28$ on the upper and lower aerofoil surfaces, respectively. This trip was not taken into account for the present simulations, where a fully turbulent flow was assumed.

Two dimensional simulations were conducted on this geometry since the original dataset was reported to be suitable for such modelling approaches[42]. The data presented in the AGARD report included corrections regarding the wind tunnel interference. Grids were built using mesh densities and refinement strategies using conclusions from preliminary grid refinement studies of the DLBA032 with flap deflection, which is summarised in Fig. 6. The conclusions of this grid refinement study, indicated that approximately 300,000 cells were sufficient to produce grid independent results for both deflected and undeflecte aileron cases. The following cases apply these findings with grids generated such that $y^+ \approx 1$ initial grid spacing in the wall normal direction is applied, as required by the $k - \omega$-type turbulence models

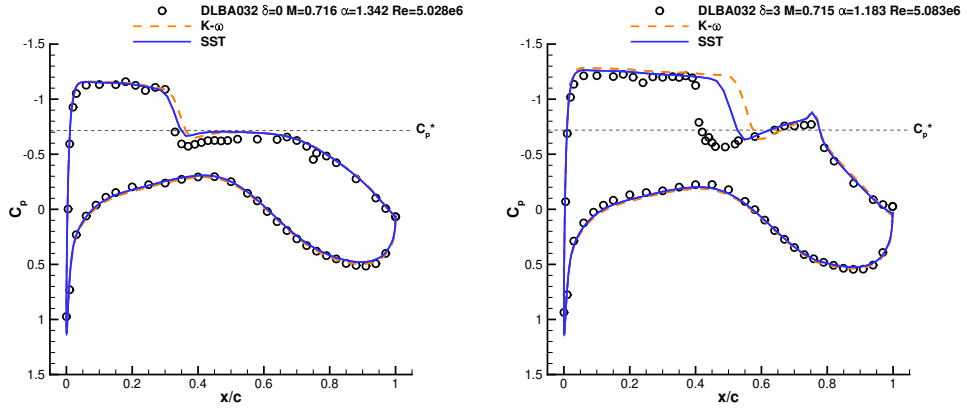


(a) Without deflection, $\alpha = 1.342°$.

(b) 3° aileron deflection, $\alpha = 1.183°$.

Figure 7: Experimental and predicted pressure distribution for the DLBA032 with and without aileron deflection at $M \approx 0.715$, $Re = 5 \times 10^6$.

employed.

Figure 7 shows the pressure distributions for the DLBA032 with an un-deflected aileron (Fig. 7a) and a deflection of 3° (Fig. 7b). Without the deflection the lower surface pressure distribution predictions agree well with the experimental data, and the shock location is within 5% chord (Fig. 7a). The upper surface suction is greater than the experiment, however the overall trend agrees. Table 1 shows that with the SST model, the change in lift is approximately 3% above the measured lift from the experiment.

With the deflected aileron, the suction near the leading edge is over-predicted, and the shock is predicted approximately 15% aft of the experiment, as shown in Fig. 7b. A similar finding was found by Londenberg[43] for $Re = 5 \times 10^6$ with a 2° aileron deflection. The agreement in the lift coefficient as shown in Table 1 is approximately 11% above the experimental data, due to the poor prediction of the shock location. It is emphasised however in the AGARD report that there is some uncertainty about the correction methods employed and that the dataset should be taken for qualitative trends[42].

Table 1: Comparing sectional lift, drag, and pitching moment behaviour of the DLBA032 at $M \approx 0.715$ and $Re \approx 5 \times 10^6$ with and without aileron deflection.

| **Configuration** | **Turbulence model** | $C_l$ | $C_d$ | $C_m$ |
|---|---|---|---|---|
| EXP $\alpha = 1.342°$ $\delta = 0°$ | | 0.7311 | 0.01044 | -0.1518 |
| CFD $\alpha = 1.342°$ $\delta = 0°$ | $k$-$\omega$ | 0.7823 | 0.0167 | -0.1614 |
| CFD $\alpha = 1.342°$ $\delta = 0°$ | SST | 0.7593 | 0.0158 | -0.1567 |
| CFD Unblown Coanda $\alpha = 1.342°$ | $k$-$\omega$ | 0.8251 | 0.0183 | -0.1710 |
| CFD Unblown Coanda $\alpha = 1.342°$ | SST | 0.8071 | 0.0175 | -0.1672 |
| EXP $\alpha = 1.183°$ $\delta = 3°$ | | 0.8931 | 0.01416 | -0.1787 |
| CFD $\alpha = 1.183°$ $\delta = 3°$ | $k$-$\omega$ | 1.0460 | 0.0236 | -0.2073 |
| CFD $\alpha = 1.183°$ $\delta = 3°$ | SST | 0.9942 | 0.0221 | -0.1962 |

# 5.0 EVALUATION OF COANDA DESIGNS IN TRANSONIC FLOW

The DLBA032 was modified to include a Coanda device by increasing the thickness of the trailing edge along the camber line. The rear 30% of the aerofoil was thickened symmetrically around the camber line, changing the trailing edge thickness from 0.55% in the baseline aerofoil to 1.23% to accommodate a Coanda surface. Figure 8 shows the modified aerofoil geometry with a CC device.

The first CC device considered used a circular Coanda surface with a 0.5% chord radius and 0.05% chord slot height (10:1 Coanda radius to slot height ratio). The design allowed for slots on the upper and lower surface, however the current investigations use upper slot blowing exclusively, see inset Fig. 8. Between the slot and upper surface of the aerofoil, a thickness of $t = 0.06\%$ chord was applied as a skin thickness. This skin thickness was maintained for all subsequent shape modifications to ensure comparisons between geometries which were not affected by a change in this parameter.

This sensitivity study considers four different Coanda designs to evaluate the effects of shock boundary layer interactions and the radius of curvature induced detachment of the jet. To assess the influence of the curvature at the slot exit, a Coanda geometry was designed with a larger Coanda radius to slot height ratio (21:1). Converging and converging-diverging nozzles were used to assess the effects of underexpanded and fully expanded Coanda jets on CC. In addition, a stepped geometry with a converging nozzle was investigated to assess whether findings by Gregory-Smith and Carpenter[8,9] can be applied to CC with a transonic freestream. The descriptions of the Coanda devices used in this study are summarised in Table 2 and Fig. 9, all other geometric features remain the same between the four designs.

To establish that the modifications made to the DLBA032 did not significantly change the behaviour of the aerofoil, the unblown case was compared with the un-deflected aileron over a range of angles of attack. Figure 10 shows the pressure coefficients and drag polars for the DLBA032 without aileron deflection and with an unblown CC device fitted as shown in Fig. 8. The shock position of the CC geometry is slightly further aft which induces greater lift than the original shape as shown in Table 1. The shape of the lift-drag polar in Fig. 10b suggests that the effects of the thickened trailing edge and CC device are small, with an approximate 0.001 increase in the drag coefficient. However the characteristics of the lift-drag polar from the original aerofoil geometry were effectively maintained.

Each CC case considered below was simulated at a freestream value of $\alpha = 1.342°$, $M_\infty = 0.716$ and $Re = 5.028 \times 10^6$.

## 5.1 Grid Refinement

Four grids were built with cell counts between approximately 100,000 and 900,000. Each finer grid was uniformly refined across the entire domain. An initial grid spacing of $y^+ \approx 1$

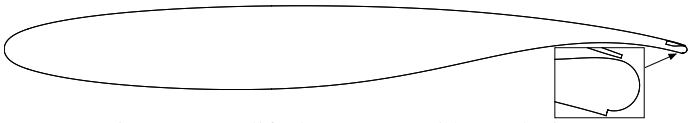

Figure 8: Modified geometry with CC device.

Table 2: Trailing edge device details (dimensions in % chord).

| CC Device | Radius ($r$) | Slot Height ($h$) | Step Height ($s$) | Skin ($t$) | Nozzle Type |
|---|---|---|---|---|---|
| 10:1 Convg | 0.500% | 0.050% | 0.000% | 0.060% | Converging |
| 21:1 Convg | 0.525% | 0.025% | 0.000% | 0.060% | Converging |
| 21:1 Condi7 | 0.525% | 0.025% | 0.000% | 0.060% | Converging–diverging designed for NPR=7 |
| 20:1:1 Step | 0.500% | 0.025% | 0.025% | 0.060% | Converging with step |

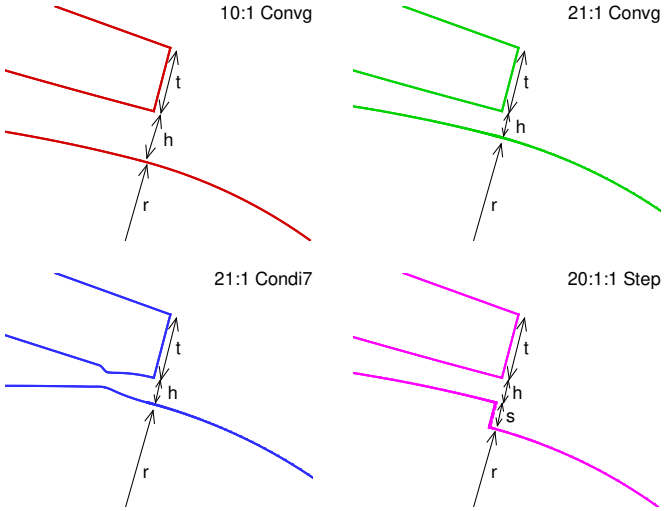


Figure 9: Diagrams of trailing edge devices.

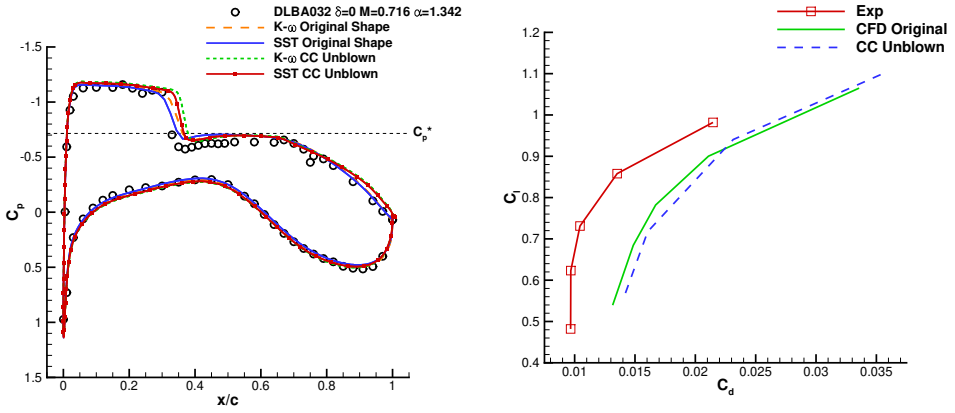


(a) Pressure coefficients.

(b) Lift-drag polar using simulations from the standard $k$-$\omega$ model.

Figure 10: Comparing unblown CC DLBA032 with original shape without aileron deflection.

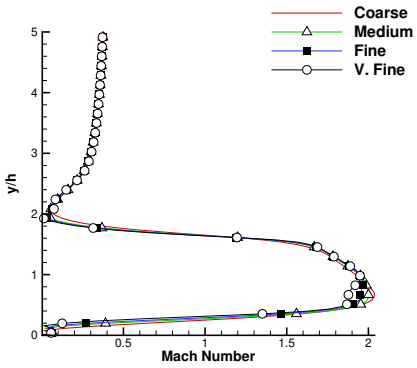


(a) Mach profile normal to Coanda surface at $3.0h$ from the slot exit.

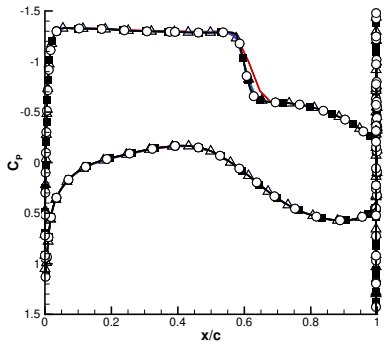


(b) Coefficient of surface pressure on the aerofoil surface.

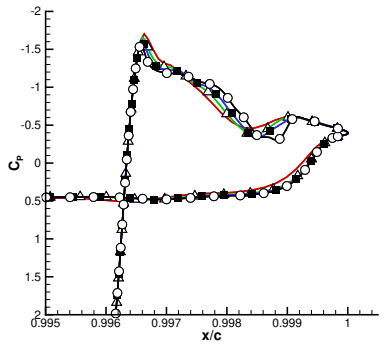


(c) Coefficient of surface pressure on the Coanda surface.

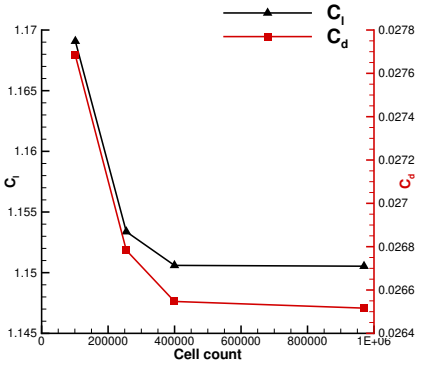


(d) $C_l$ and $C_d$

Figure 11: Effect of grid refinement on the 21:1 Coanda device at $NPR = 4.0$.

in the wall normal directions was used for all grids, where $y^+$ was calculated based on the freestream Reynolds number. For a circular Coanda shape with a 21:1 radius to slot height ratio, the effect of grid refinement on the lift and drag on the aerofoil was assessed at the conditions described above with blowing at $NPR = 4.0$

Figure 11 shows the effect of the grid size on the DLBA032 section with CC. Figure 11a shows the Mach profile of the jet and aerofoil boundary layer at the trailing edge, taken $3.0h$ from the slot exit. Minor differences occur in the jet profiles between the "Fine" and "V. Fine" grids with 400,000 and 900,000 cells, respectively. These differences, however, do not have a significant effect on the surface pressures on the Coanda nor the main aerofoil surface (Figs. 11b and 11c). As a result the Fine grid is within 0.01% of the lift and 0.1% of the drag coefficients from the solution using the finest grid (V.Fine on Fig. 11), as shown in Fig. 11d, suggesting that the 400,000 cell grid produces sufficiently grid-independent results.

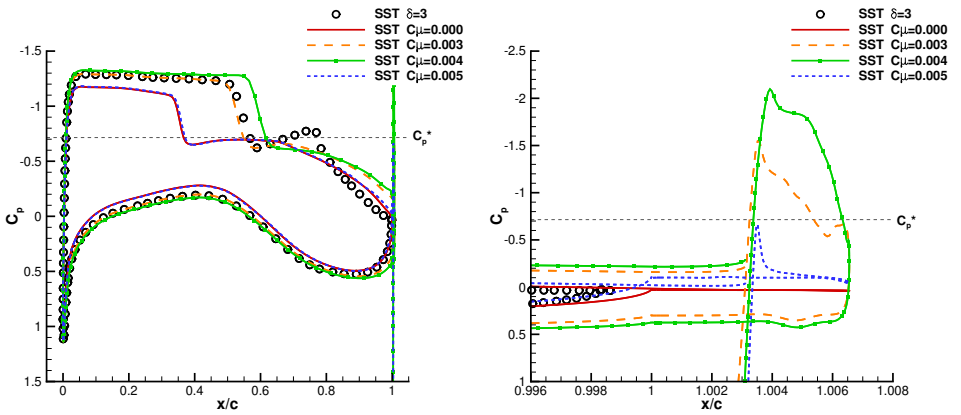


Figure 12: Predicted pressure coefficients for Douglas DLBA032 at $\alpha = 1.342°$, $M = 0.716$ and $Re = 5.028 \times 10^6$ for an aileron deflection and with blowing at $C_\mu \approx 0.003$, $C_\mu \approx 0.004$ and $C_\mu \approx 0.005$ for the 10:1 configuration. Symbols here represent the simulated pressure distribution of the deflected aileron case at the same freestream conditions and turbulence model.

### 5.2 Converging nozzle with 10:1 radius to slot ratio (10:1 Convg)

The simulated pressure coefficients for the DLBA032 aerofoil with a circular Coanda device with 10:1 radius to slot ratio are compared with an aileron deflection of 3° in Fig. 12. As with the NASA 6% elliptical CC aerofoil results, the shock moves aft with blowing which is consistent with an increase in lift and circulation. The symbols in Fig. 12 represent the simulated results of the aileron deflection case at the same conditions.

Comparing the predicted results of the aileron deflection and blowing over the 10:1 configuration at $C_\mu = 0.003$, the lower surface and the front section of the aerofoil have similar pressure distributions. The rear section of the aerofoil with blowing has more suction, and does not have the characteristic peak in suction at the hinge line. This additional suction towards the trailing edge generates an increase in the 'nose down' pitching moment compared to that of a 3° aileron, Fig. 13.

With increased blowing, the sectional lift, drag and pitching moment coefficients on the aerofoil increase. Figure 13 shows the behaviour of the loads due to blowing, also shown are predicted loads for the aerofoil at a range of aileron deflection angles. At a similar lift coefficient to that of a deflected aileron of 3°, blowing over the 10:1 configuration at $C_\mu = 0.003$ resulted in a smaller drag increase.

Additional blowing results in separation of the jet from the Coanda surface, due to the increased underexpansion of the jet. For $C_\mu = 0.004$ the jet separated from the Coanda surface, however in this case the jet re-attached to the surface. This re-attachment may be due to the low pressure within the separated bubble, as shown in Fig. 14a. In Fig. 14b, Mach contours using a moderately higher blowing rate of $C_\mu = 0.005$ are shown, where the jet is detached. The shock impinging on the Coanda surface is too strong for the flow to re-attach to the Coanda. As seen in Fig. 14b, the separation bubble does not form and so the mechanism to re-attach the jet is not present.

The lift characteristics for blowing at $C_\mu = 0.003$ suggest that it is possible to replicate the lift achieved with a 3° aileron deflection using CC in this flight regime, with a reduction in the drag and an increase in the pitching moment, as shown in Fig. 13. For this configuration, a blowing rate of $C_\mu = 0.005$ caused detachment of the jet. While the jet remains attached, a lift augmentation ratio of $\Delta C_l/C_\mu = 84$ was achieved.

### 5.3 Converging nozzle with 21:1 radius to slot ratio (21:1 Convg)

The effect of changing the slot height to radius ratio was investigated by halving the slot height of the 10:1 Coanda trailing edge device, resulting in a surface with a radius and slot height of 0.525% and 0.025% chord lengths respectively, and a 21:1 Coanda radius to slot ratio. Using the plenum pressure ratio of 5.0 was found to detach the jet from the 10:1 geometry, while with the 21:1 radius the jet remained attached.

Figure 13 shows that at $C_\mu = 0.002$ (NPR=4.0), the SST predictions gave comparable performance to the converging nozzle over the 10:1 surface at $C_\mu = 0.003$ (NPR=3.0) and also the aileron deflection of 3°. For the same blowing rate, the 21:1 device produced approximately 50% higher lift augmentation ratio than the 10:1 CC device, resulting in a $\Delta C_l/C_\mu = 134$.

Similarly to the 10:1 configuration, further blowing detached the jet due to the strongly under-expanded jet flow at $C_\mu = 0.0035$ (NPR=7.0).

By increasing the radius of curvature near the slot exit, the boundary layer within the jet experiences a weaker adverse pressure ratio. As a result the jet boundary layer is able to cope with a stronger shock assosciated with underexpansion at a higher pressure ratio when using the 21:1 configuration compared with the 10:1, above.

### 5.4 Converging-diverging nozzle with 21:1 radius to slot ratio (21:1 Condi7)

Bevilaqua and Lee's[26] method of characteristics approach fixes a desired irrotational vortex profile along the slot. The two dimensional characteristics equations are solved to determine the nozzle wall profiles from the slot exit to the nozzle throat for a given pressure ratio and Coanda radius. This method of characteristics procedure was applied to the nozzle walls of the 21:1 configuration to design a nozzle to perform at $NPR = 7.0$. At this pressure ratio, flow from a purely converging nozzle failed to attach, as described in Section 5.3 above. The resulting asymmetrically contoured converging-diverging nozzle is shown in Fig. 9. In designing the nozzle, the exit slot height from the 21:1 Convg device is retained at 0.025% chord. The contouring of the nozzle gave an effective throat height of 0.015% chord, resulting in an expansion ratio of 1.67. For choked conditions, this results in a reduced mass flow rate.

Figure 14c shows the converging diverging nozzle operating at the design condition $NPR = 7$. A relatively weak shock occurs at the slot exit, followed by a small separation bubble on the Coanda surface at approximately $x = 1.004$.

Although the nozzle was designed to fully expand the jet, the used method of characteristics did not account for the boundary layer. The effective nozzle contour as seen by the flow, due to the displacement thickness, was found to significantly reduce the expansion rate and so the jet was under-expanded. This can be seen from the Mach number profile at a station at the slot exit in Fig. 15, where the theoretical irrotational vortex profile is also shown. The SST model predicted a thinner boundary layer than that of the $k$-$\omega$, however both models gave a slope similar to the idealised profile at a reduced value for the mean Mach number.

For a pressure ratio of 9.0, the jet emanating from the converging-diverging nozzle under-expands, however the magnitude of under-expansion is lessened by the nozzle. This allows the jet to adhere to the Coanda surface and gives a lift increment of $\Delta C_l = 0.4077$ using the SST model. An approximate linear change in the lift and drag coefficients using the converging-diverging Coanda until $C_\mu \approx 0.004$ is shown in Fig. 13. Again, due to underexpansion, the jet eventually detached from the Coanda at $C_\mu \approx 0.006$ (NPR=13.0).

Figure 16 shows the differences between the jet profiles using the converging and the converging-diverging nozzles at $NPR = 4$ and $NPR = 7$ both with a 21:1 Coanda radius to slot height ratio. At $NPR = 4$, the $C_\mu$ of the converging nozzle was approximately 10% higher than that from the converging-diverging nozzle, however the $\Delta C_l$ was 54% higher using the converging nozzle as shown in Fig. 13. The reduction in $\Delta C_l$ at the same NPR is possibly due to the reduction in mass flow rate through the shorter throat height of the converging diverging nozzle. The underexpansion of the jet from the 21:1 Convg device appears to entrain more of the freestream than when using the 21:1 Condi7 nozzle at the same conditions. This underexpansion is an impediment at higher nozzle pressure ratios however, since it also brings about shock induced separation of the Coanda boundary layer. By expanding the flow, the extent of the separation is reduced and detachment occurs later.

Figure 14d shows contours of Mach number for an over-expanded nozzle on the DLBA032. Although the flow separated inside the nozzle, the jet remained largely attached to the Coanda surface for NPR=3.0 ($C_\mu = 0.0014$). In all over-expanded cases ($C_\mu < 0.003$) using this nozzle designed for NPR=7, a reduction in lift augmentation ratio and thus efficiency was observed. Comparing this with the same radius to slot height ratio, $\Delta C_l/C_\mu$ with 21:1 Condi7 was 75% of the augmentation ratio achieved from the convergent only nozzle 21:1 Convg.

In contrast to the other designs, the gradient of the $\Delta C_l$ vs $C_\mu$ plot for the 21:1 Condi7 in Fig. 13 initially increases as $C_\mu$ increases. Up until the design condition at $C_\mu = 0.0032$ a maximum $\Delta C_l/C_\mu = 105$ was found. Following from the design point, the slope of $\Delta C_l$ vs $C_\mu$ begins to diminish.

### 5.5 Converging nozzle with a 20:1:1 radius to slot to step ratio (20:1:1 Step)

Using the initial 21:1 purely converging configuration as described above (Section 5.3), the radius of the Coanda was decreased by 0.025% chord to give a radius of slot height of 0.5% chord while maintaining the 0.025% chord slot height. This produced a step between the exit of the converging nozzle and the Coanda surface.

Figure 14e shows the behaviour of the under-expanded jet at $C_\mu = 0.0027$, the shock cell structure can be seen which begins to follow the Coanda surface. At $NPR = 7$ ($C_\mu = 0.0035$), the flow from the same nozzle caused the jet to detach from the 21:1 configuration (described above), while including the step promoted attachment to the Coanda surface. Attachment of the jet remains up to $NPR = 11.0$ ($C_\mu = 0.0057$). As shown in Fig. 13, the behaviour of the jet over the stepped Coanda follows the same behaviour as that of the converging-diverging nozzle. A maximum $\Delta C_l/C_\mu = 108$ up to $C_\mu = 0.0038$ was found when using the stepped Coanda. Below the design point of the 21:1 Condi7 nozzle, the stepped geometry gave a greater $\Delta C_l/C_\mu$. At $NPR = 11.0$, the jet underexpands such that a shock boundary layer interaction with the Coanda is strong enough to separate the jet, despite the step (Fig. 14f).

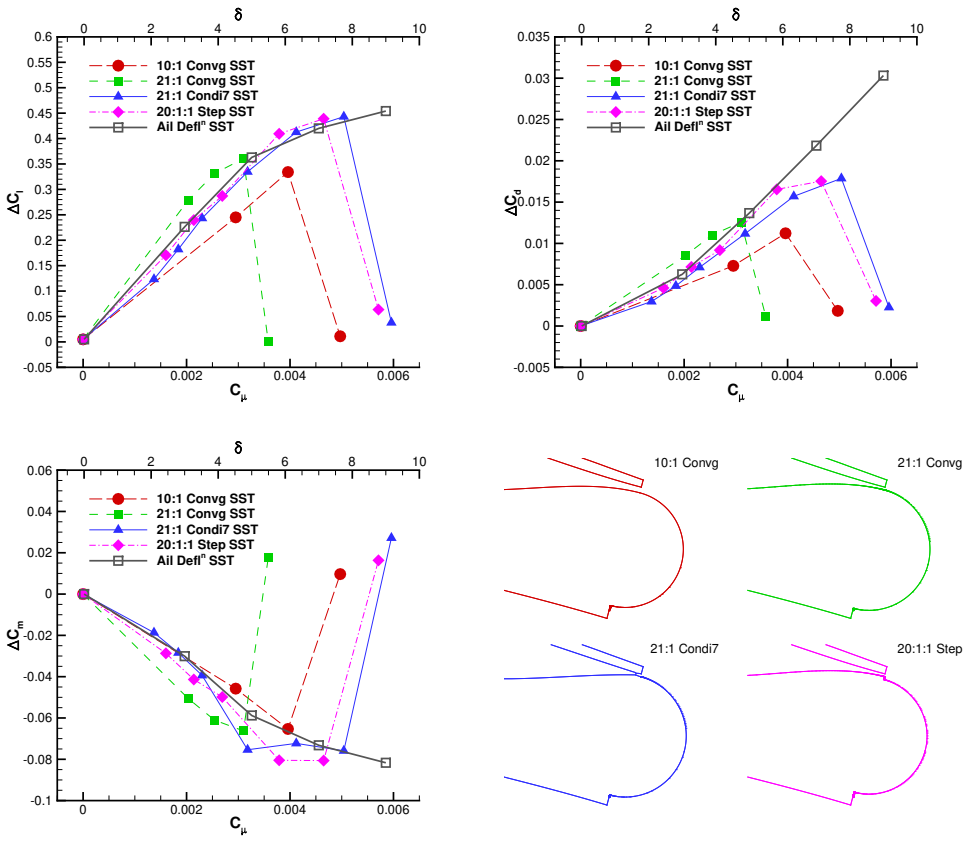


Figure 13: Comparing lift, drag and pitching moment coefficient characteristics with blowing over various Coanda surfaces against aileron deflection on the DLBA032 at $M = 0.716$, $\alpha = 1.342°$ and $Re = 5.028 \times 10^6$.

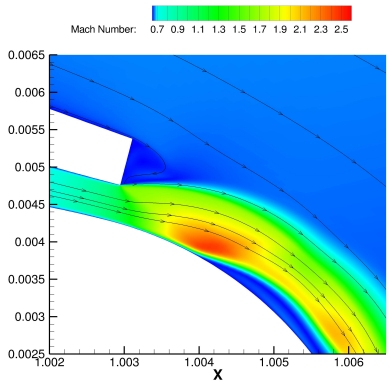


(a) 10:1 circular Coanda with converging nozzle, NPR=4. $C_\mu = 0.0040$.

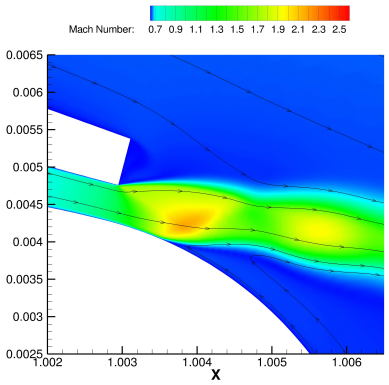


(b) 10:1 circular Coanda with converging nozzle, NPR=5. $C_\mu = 0.0050$.

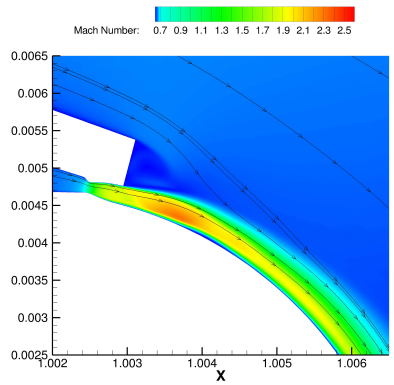


(c) 21:1 circular Coanda with con-di nozzle designed for NPR=7, at design. $C_\mu = 0.0032$.

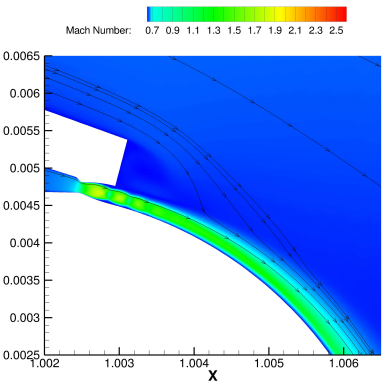


(d) 21:1 circular Coanda with con-di nozzle designed for NPR=7, NPR=3. $C_\mu = 0.0014$.

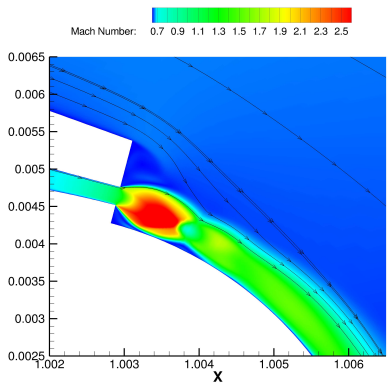


(e) 20:1:1 circular Coanda with step and converging nozzle, NPR=5. $C_\mu = 0.0027$.

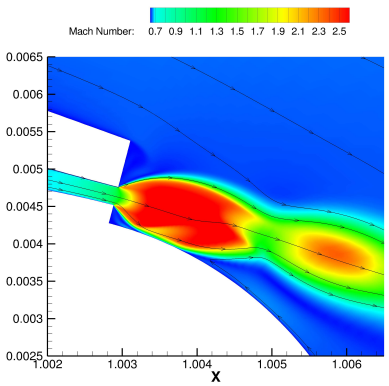


(f) 20:1:1 circular Coanda with step and converging nozzle, NPR=11. $C_\mu = 0.0057$.

Figure 14: Contours of Mach number for various Coanda designs using the $k$-$\omega$ SST turbulence model.

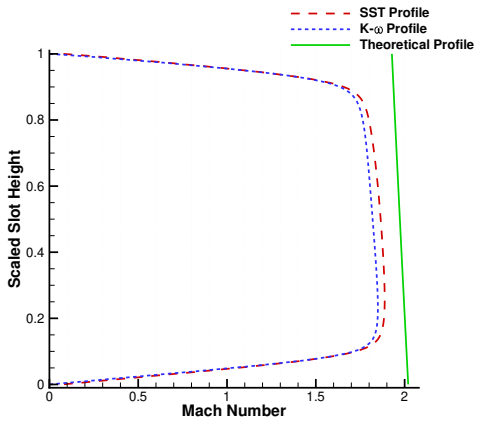


Figure 15: Profile of mach numbers for the SST and $k$-$\omega$ models at the slot exit for the converging diverging configuration with a 21:1 radius to slot ratio at design condition for blowing at PR7.

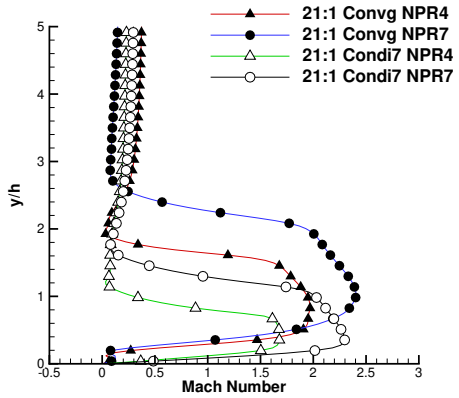


Figure 16: Mach profile normal to Coanda surface at 3.0$h$ from the slot exit.

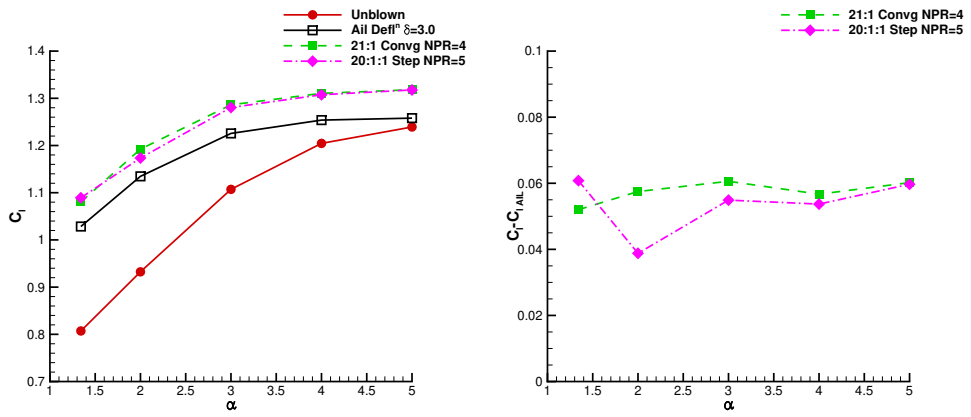


(a) $C_l$ (b) $\Delta C_l$ with respect to the aileron deflection.

Figure 17: Effect of angle of attack on $C_l$ at $M = 0.716$ and $Re = 5 \times 10^6$.

## 5.6 Effect of angle of attack

To assess the range of operability of CC in transonic flow, two representative CC cases are compared here with a deflected aileron case. The effect of increasing shock strength on the upper surface of the aerofoil is investigated by operating at steeper angles of attack. Figure 17 shows the effect of varying the angle of attack on the lift characteristics of CC and a 3° aileron deflection. The two CC cases shown are the 21:1 Convg and the 20:1:1 Step running at $C_\mu = 0.0020$ and $C_\mu = 0.0027$, respectively. Independent of trailing edge geometry each case undergoes a stall as $\alpha$ increases, due to the stronger shock on the upper surface causing the boundary layer to separate and so a progressively smaller $\Delta C_l$ as $\alpha$ increased. This gradual reduction in $\Delta C_l$ is due to a strong shock wave separating the boundary layer on the upper surface of the aerofoil. The rate at which $\Delta C_l$ degraded was approximately constant between the CC and aileron deflection cases as shown in Fig. 17b, where the difference between circulation control cases and the 3° aileron are presented. These results suggest that the behaviour of CC is similar to that of a deflected aileron at the higher angles of attack considered. At higher angles of attack, degredation of the mean flow rather than the CC system appears to be the limiting factor in retaining control of the forces and moments. Such a result may mean that the well understood principles of using ailerons in transonic flows could be applied to the use of CC.

Figure 18 shows the effect of the aileron deflection and CC have on the flowfield at the trailing edge of the aerofoil. In both cases a strong shock boundary layer interaction occured at approximately 55% chord, with the shock further aft for the CC case from the increased circulation generating additional lift. With CC the trailing edge separation is reduced in severity due to the additional boundary layer momenentum from jet entrainment and a favourable pressure gradient due to blowing. Although not investigated here, it may be possible that CC may offer some shock buffet onset alleviation.

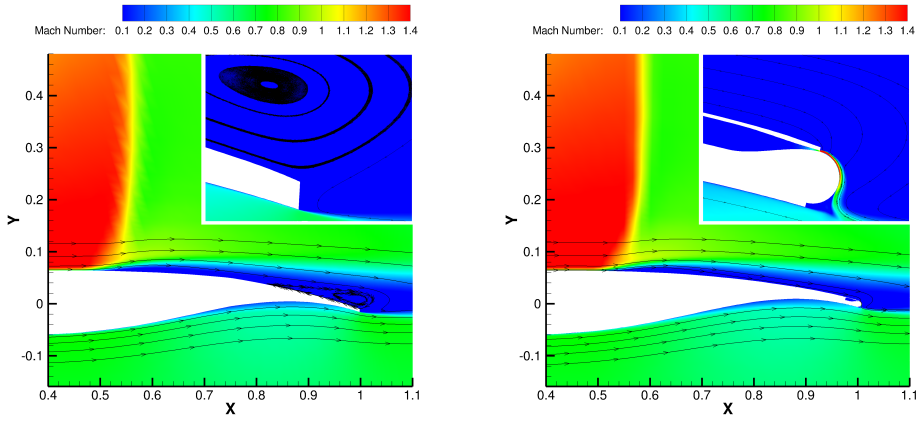


(a) 3° aileron deflection.

(b) 21:1 Convg at NPR=4.

Figure 18: Mach contours at the trailing edge of aileron deflection and CC cases at $\alpha = 5°$, $M = 0.716$ and $Re = 5 \times 10^6$. Inset shows detail of the trailing edges, at the same scale in both images.

### 5.7 Summary of results

An increase in the ratio between the radius of curvature and the slot height increased the CC effectiveness by providing an increase in total lift and also the lift augmentation ratio. This finding is in line with conclusions from experimental studies described in Section 2, where the local radius of curvature at the slot exit was increased by altering the eccentricity of elliptical Coanda devices[6,2]. Here we have shown that an increase in the ratio between the Coanda radius and slot height resulted in an increase in overall lift achievable.

The limiting detachment pressure ratio can be extended by using a suitably designed converging-diverging nozzle. In the cases considered in this paper, the converging-diverging nozzle was designed for the operating condition for which the jet detached using a convergent only Coanda device at the same radius to slot height ratio. Further extension may be possible by designing the converging-diverging nozzle for higher pressure ratios, however a further reduction in efficiency is likely be observed.

Introducing a step between the Coanda surface and the slot exit also promoted a delay in detachment for CC with a transonic freestream. This was due to the shock boundary layer interaction being replaced by a shock shear interaction. For very highly underexpanded stepped Coanda jets, the reattachment shock was the cause of separation.

As shown in Fig. 13 each of the designs can be compared to an aileron deflection angle, the 10:1 Convg and 21:1 Convg devices achieved a maximum $\Delta C_l$ equivalent to that of approximately 4° and 5° aileron deflection, respectively. Both converging-diverging and stepped devices gave an equivalent aileron deflection of approximately $7.5 - 8°$ before detachment.

# 6.0 CONCLUSIONS AND FUTURE WORK

The current work investigated the simulation of transonic CC for the supercritical DLBA032 aerofoil section. Results showed how, for a supercritical section in transonic conditions, fluidic circulation control can achieve similar performance as the aileron with moderate deflection angles.

The design study involved different nozzles, nozzle exit geometries and Coanda surfaces to investigate which design performs most consistently over a range of blowing coefficients. It was found that replicating the lift, drag and moment characteristics of a 25% chord aileron at $\delta = 4.0^\circ$ is possible with a converging nozzle and a Coanda radius to slot height ratio of 10:1. However, a wider range of operating pressure ratios was found for a 21:1 ratio. For the converging nozzle the limiting factor is the strong shock-induced separation created by the under-expansion of the nozzle flow.

The results for converging-diverging nozzles showed that, as expected, the under-expansion related shock-induced separation can be delayed to higher pressure ratios. Furthermore, for the converging nozzle, it was found that the shock-induced separation can be delayed by applying a small step in the geometry between the nozzle exit and the Coanda surface. It was shown that using either the converging-diverging or the stepped Coanda geometry can perform equivalently to an aileron deflection angle of up to $8^\circ$.

The effects of angle of attack were in addition considered with a comparison between circulation control and a $3^\circ$ deflected aileron. The performance of the CC devices at a constant blowing rate performed similarly to the deflected aileron. Each device considered lost effectiveness at the same rate, due to the mean flow and upper surface boundary layer separating from a strong shock boundary layer interaction.

The present study did not investigate the effects of different slot heights, nor a converging–diverging CC device with a step. Further work regarding these design choices is ongoing. In addition, an investigation into the effectiveness of the sizing of Coanda devices in transonic flows is recommended for future studies. In doing so it may be possible to minimise further the drag penalty due to the bluntness of the Coanda device.

For the Coanda device to replace flaps and ailerons completely, the system must be able to operate over the full flight regime, including take–off and landing and blowing over the lower Coanda surface. It is recommended that future studies would focus on actuation for all flight conditions and manoeuvre requirements, including the use of CC as a yaw control effector. Full system analysis to include the necessary air supply and its effects on engine bleed air and vehicle weight should form part of a future integration study. For the system to be considered for use on an aircraft, the effect of failure of one or more Coanda devices should be investigated. Initial tests may possibly include the combined use of flaps and CC devices, however this would result in an increase of weight. The design and integration of fluidic control devices such as CC via the Coanda effect are currently being studied as part of the NATO Science and Technology Organisation task group, AVT-239[44].

# ACKNOWLEDGEMENTS

The present research was supported by a doctoral scholarship from the Engineering and Physical Sciences Research Council of the UK, with additional sponsorship from BAE Systems and DSTL through the industrial CASE Award scheme.

## REFERENCES


1. PATERSON, E. G., BAKER, W. J., KUNZ, R. F. AND PELTIER, L. J., Rans and detached-eddy simulation of the nccr airfoil, *31st Annual International Symposium on Computer Architecture*, 2004, pp. 112–122.
2. ALEXANDER, M. G., ANDERS, S. G., JOHNSON, S. K., FLORANCE, J. P. AND KELLER, D. F., Trailing edge blowing on a two-dimensional six-percent thick elliptical circulation control airfoil up to transonic conditions, Tech. Rep. TM-2005-213545, NASA, 2005.
3. CARPENTER, P. W. AND GREEN, P. N., The aeroacoustics and aerodynamics of high-speed coanda devices, part 1: Conventional arrangement of exit nozzle and surface, *Journal of Sound and Vibration*, Vol. 208, No. 5, 1997, pp. 777–801.
4. SAWADA, K. AND ASAMI, K., Numerical study on the underexpanded coanda jet, *Journal of Aircraft*, Vol. 34, No. 5, 1997, pp. 641–647.
5. ABRAMSON, J. AND ROGERS, E. O., High speed characteristics of circulation control airfoils, *AIAA 21st Aerospace Sciences Meeting*, AIAA, 1983, p. 265.
6. ENGLAR, R. J., Two-dimensional transonic wind tunnel tests of three 15-percent thick circulation control airfoils, Tech. Rep. AD882075, DTNSRDC, 1970.
7. SCHLECHT, R. AND ANDERS, S. G., Parametric evaluation of thin, transonic circulation-control airfoils, *45th AIAA Aerospace Sciences Meeting*, Vol. 5, 8th-11th January 2007, pp. 3374–3398.
8. CARPENTER, P. W. AND SMITH, C., The aeroacoustics and aerodynamics of high-speed coanda devices, part 2: Effects of modifications for flow control and noise reduction, *Journal of Sound and Vibration*, Vol. 208, No. 5, 1997, pp. 803–822.
9. GREGORY-SMITH, D. G. AND SENIOR, P., The effects of base steps and axisymmetry on supersonic jets over coanda surfaces, *International Journal of Heat and Fluid Flow*, Vol. 15, No. 4, 1994, pp. 291–298.
10. JONES, G. S., YAO, C. S. AND ALLAN, B. G., Experimental investigation of a 2d supercritical circulation-control airfoil using particle image velocimetry, *3rd AIAA Flow Control Conference*, Vol. 1, 5th-8th June 2006, pp. 367–386.
11. VON GLAHN, U. H., Use of the coanda effect for jet deflection and vertical lift with multiple-flat-plate and curved-plate deflection surfaces, Tech. Rep. TN-4377, NACA, 1958.
12. DVORAK, F. A. AND CHOI, D. H., Analysis of circulation-controlled airfoils in transonic flow, *Journal of Aircraft*, Vol. 20, No. 4, 1983, pp. 331–337.
13. COULURIS, G. J., SIGNOR, D. AND PHILLIPS, J., Cruise-efficient short takeoff and landing (cestol): Potential impact on air traffic operations, Tech. Rep. CR-2010-216392, NASA, 2010.
14. COOK, M. V., BUONANNO, A. AND ERBSLÖH, S. D., A circulation control actuator for flapless flight control, *Aeronautical Journal*, Vol. 112, No. 1134, 2008, pp. 483–489.
15. LIN, J. C., ANDINO, M. Y., ALEXANDER, M. G., WHALEN, E. A., SPOOR, M. A., TRAN, J. T. AND WYGNANSKI, I. J., An overview of active flow control enhanced vertical tail technology development, *54th AIAA Aerospace Sciences Meeting, AIAA SciTech,(AIAA 2016-0056)*, 2016, p. 56.

16. Whalen, E., Shmilovich, A., Spoor, M., Tran, J., Vijgen, P., Lin, J. and Andino, M., Flight test of an afc enhanced vertical tail, *8th AIAA Flow Control Conference*, 2016.

17. Abramson, J., Two-dimensional subsonic wind tunnel evaluation of two related cambered 15-percent thick circulation control airfoils, Tech. Rep. ASED-373, DTNSRDC, 1977.

18. Wetzel, D. A., Griffin, J. and Cattafesta III, L. N., Experiments on an elliptic circulation control aerofoil, *Journal of Fluid Mechanics*, Vol. 730, 2013, pp. 99–144.

19. Nishino, T., Hahn, S. and Shariff, K., Large-eddy simulations of a turbulent coanda jet on a circulation control airfoil, *Physics of Fluids*, Vol. 22, No. 12, 2010.

20. Englar, R. J., Jones, G. S., Allan, B. G. and Lin, J. C., 2-d circulation control airfoil benchmark experiments intended for cfd code validation, *47th AIAA Aerospace Sciences Meeting Including the New Horizons Forum and Aerospace Exposition*, 5th-8th January 2009, p. 902.

21. Wilkerson, J. B. and Montana, P. S., Transonic wind tunnel test of a 16-percent-thick circulation control airfoil with one-percent asymmetric camber, Tech. Rep. ASED-82/03, DTNSRDC, 1982.

22. Wood, N. J. and Conlon, J. A., Performance of a circulation control airfoil at transonic speeds, *AIAA 21st Aerospace Sciences Meeting.*, AIAA, 10th-13th January 1983, p. 83.

23. Pulliam, T. H., Jespersen, D. C. and Barth, T. J., Navier-stokes computations for circulation control airfoils, *Von Karman Inst. for Fluid Dynamics Numerical Techniques for Viscous Flow Calculations in Turbomachinery Bladings*, Vol. 1, No. N86-30988, 1986, pp. 22–34.

24. Swanson, R. C., Rumsey, C. L. and Anders, S. G., Aspects of numerical simulation of circulation control airfoils, *AIAA Progress in Astronautics and Aeronautics*, Vol. 214, 2006, pp. 469–498.

25. Cornelius, K. C. and Lucius, G. A., Physics of coanda jet detachment at high-pressure ratio, *Journal of Aircraft*, Vol. 31, No. 3, 1994, pp. 591–596.

26. Bevilaqua, P. M. and Lee, J. D., Design of supersonic coanda jet nozzles, *NASA. Ames Research Center Proceedings of the Circulation-Control Workshop*, NASA, 01 May 1987, pp. 289–312.

27. Gregory-Smith, D. G. and Gilchrist, A. R., The compressible coanda wall jet-an experimental study of jet structure and breakaway, *International Journal of Heat and Fluid Flow*, Vol. 8, No. 2, 1987, pp. 156–164.

28. Steijl, R., Barakos, G. and Badcock, K., A Framework for CFD Analysis of Helicopter Rotors in Hover and Forward Flight, *Int. J. Numer. Meth. Fluids*, Vol. 51, 2006, pp. 819–847.

29. Steijl, R. and Barakos, G., Sliding Mesh Algorithm for CFD Analysis of Helicopter Roto-Fuselage Aerodynamics, *Int. J. Numer. Meth. Fluids*, Vol. 58, 2008, pp. 527–549.

30. Badcock, K., Richards, B. and Woodgate, M., Elements of computational fluid dynamics on block structured grids using implicit solvers, *Progress in Aerospace Sciences*, Vol. 36, 2000, pp. 351–392.

31. Barakos, G., Steijl, R., Badcock, K. and Brocklehurst, A., Development of CFD Capability for Full Helicopter Engineering Analysis., 31st European Rotorcraft Forum, 13-15

September 2005, Florence, Italy, 2005.

32. CARRIÓN, M., WOODGATE, M., STEIJL, R., BARAKOS, G., GOMEZ-IRADI, S. AND MUNDUATE, X., Understanding wind-turbine wake breakdown using computational fluid dynamics, *AIAA Journal*, Vol. 53, No. 3, 2014, pp. 588–602.
33. LAWSON, S. AND BARAKOS, G., Evaluation of des for weapons bays in ucavs, *Aerospace Science and Technology*, Vol. 14, No. 6, 2010, pp. 397–414.
34. HOHOLIS, G., STEIJL, R. AND BADCOCK, K., Circulation control as a roll effector for unmanned combat aerial vehicles, *Journal of Aircraft*, Vol. 53, No. 6, 2016, pp. 1875–1889.
35. WILCOX, D. C., Reassessment of the scale-determining equation for advanced turbulence models, *AIAA Journal*, Vol. 26, No. 11, Jan-1 1988, pp. 1299–1310.
36. MENTER, F. R., Two-equation eddy-viscosity turbulence models for engineering applications, *AIAA Journal*, Vol. 32, No. 8, Jan-1 1994, pp. 1598–1605.
37. WILCOX, D. C., Formulation of the k-$\omega$ turbulence model revisited, *AIAA Journal*, Vol. 46, No. 11, 2008, pp. 2823–2838.
38. SPALART, P. AND ALLMARAS, S. R., One-equation turbulence model for aerodynamic flows, *Recherche aerospatiale*, Jan-1 1994, pp. 5–21.
39. WALLIN, S. AND JOHANSSON, A. V., An explicit algebraic reynolds stress model for incompressible and compressible turbulent flows, *Journal of Fluid Mechanics*, Vol. 403, 2000, pp. 89–132.
40. GRIGORIEV, I. A., WALLIN, S., BRETHOUWER, G. AND JOHANSSON, A. V., A realizable explicit algebraic reynolds stress model for compressible turbulent flow with significant mean dilatation, *Physics of Fluids (1994-present)*, Vol. 25, No. 10, 2013.
41. MIN, B. Y., LEE, W., ENGLAR, R. AND SANKAR, L. N., Numerical investigation of circulation control airfoils, *Journal of Aircraft*, Vol. 46, No. 4, 2009, pp. 1403–1410.
42. ELSENAAR, A., WAGGONER, E. G. AND ASHILL, P. R., A selection of experimental test cases for the validation of cfd codes, Tech. Rep. AR-303, AGARD, 1994.
43. LONDENBERG, W., Turbulence model evaluation for the prediction of flows over a supercritical airfoil with deflected aileron at high reynolds number, *31st Aerospace Sciences Meeting and Exhibit*, AIAA, 11–14 Jan 1993, p. 191.
44. NATO, Avt-239 innovative control effectors for manoeuvring of air vehicles, `https://www.cso.nato.int/ACTIVITY_META.asp?ACT=4343`, 2013, Accessed: 15th Dec 2015.